Springer

KSME

Journal of Mechanical Science and Technology 32 (10) (2018) 4711~4720
www.springerlink.com/content/1738-494x(Print)/1976-3824(Online)
DOI 10.1007/s12206-018-0918-x

An experimental study on the cavitation vibration characteristics of a centrifugal pump at normal flow rate †

Yi Li[1], Guangwei Feng[1], Xiaojun Li[1,*], Qiaorui Si[2] and Zuchao Zhu[1]

[1]*Key Laboratory of Fluid Transmission Technology of Zhejiang Province, Zhejiang Sci-Tech University, Hangzhou 310018, China*
[2]*National Research Center of Pumps, Jiangsu University, Zhenjiang 212013, China*

(Manuscript Received February 21, 2018; Revised May 23, 2018; Accepted June 18, 2018)

Abstract

Cavitation is a challenging flow abnormality that leads to undesirable effects on the energy performance of the centrifugal pump and the reliable operation of the pump system. The onset and mechanism of a phenomenon that results in unsteady cavitation must be realised to ensure a reliable operation of pumps under the cavitation state. This study focuses on cavitation instability at normal flow rate, at which point the unsteady cavitation occurs as the available net positive suction head (NPSHa) falls below 5.61 m for the researched pump. An ameliorative algorithm–united algorithm for cavitation vibration analysis is proposed on the basis of short time Fourier transform (STFT) and Wigner–Ville distribution (WVD). The STFT–WVD method is then tested using vibration data measured from the centrifugal pump. The relationship between vibration and suction performance indicates that the inception and development of cavitation can be effectively detected by the distribution and intensity of the united algorithm at the testing points. Intermediate frequency components at approximately 6 kHz fluctuate initially with the development of cavitation. A time–frequency characteristic is found to be conducive to monitoring the cavitation performance of centrifugal pumps.

Keywords: Centrifugal pump; Cavitation; Vibration characteristic; Time–frequency analysis; Energy performance

1. Introduction

Cavitation is a common physical phenomenon in pumps and is defined as the formation process of the vapour phase in a liquid when subjected to low pressures [1, 2]. Generally, cavitation poses a threat to the system, if a pump operates under cavitation conditions, the vapour gradually fills the spaces inside the impeller passage along the blades, whilst the pressure of the pump suction decreases. The cavity volume increases rapidly when the suction pressure decreases to a certain value, normal energy transformation inside the pump is disturbed, and fatal failure in pump energy performance is induced [3-7]. Cavitation can also produce high levels of noise and vibration which can lead to erosive damage on the pump surface. Thus, ensuring a reliable pump operation under the cavitation state requires an understanding of incipient cavitation and the development of cavitation within pumps.

The cavitation process can be summarized as incipient cavitation, quasi-steady cavitation, and unsteady cavitation with the reduction in pressure [8, 9]. In detecting cavitation, the variables such as pressure, flow rate and motor power, related to the hydraulic performance of a pump can be monitored. In the work of Lu [10, 11], dynamic pressure sensors were used to measure transient pressure at the inlet and outlet of a pump to detect cavitation. Chudina [12] experimentally determined a fixed discrete frequency that correspond to the induced noise of a centrifugal pump and explored the cavitation inception detection and identification method based on wavelet entropy. Ashokkumar [13], Han [14], and Christopher [15] discussed the cavitation noise induced by numerous experimental studies and put forward the corresponding numerical algorithms. Faisal [16] extracted the fault features from a stator current spectrum; these features are related to a specific fault frequency to detect cavitation, blockage and damage of impeller. Harihara et al. [17] designed a fault detection system based on a model of the system which is used to monitor the cavitation state.

Vibration signal processing has also been investigated to monitor cavitation [18, 19] and the frequency spectrum of a vibration signal is a common method for analyzing the cavitation phenomenon [20]. However, the conventional Fourier process is inappropriate given the random and discrete nature of the cavitation process. For non-stationary signals, the frequency spectrum cannot determine the transformation of frequency components. Thus, distinguishing the manner by

*Corresponding author. Tel.: +86 571 86843348, Fax.: +86 571 86843348
E-mail address: lixj@zstu.edu.cn
† Recommended by Associate Editor Sangyoup Lee

which the instantaneous frequency of vibration signals varies with time is difficult. An analysis of the vibration signals of cavitation based on the time–frequency characteristics is a suitable method [21]. Hodkiewicz [22] used a short-time Fourier transform (STFT) to illustrate the manner by which the frequency contributions within the vibration signals change with time. The STFT method is more progressive in achieving time resolution than the traditional method. However, the time–frequency aggregation of the STFT is limited, thereby leading to the emergence of wavelet transform. Pavesi et al. [23, 24] demonstrated the applicability of wavelets in the turbomachinery field. However, selecting a proper basic wavelet for wavelet transform is challenging. Thus, applying wavelet transform in analyzing vibration signals is limited.

In this study, the correlation between cavitation characteristics and vibration signals was investigated to identify and characterize the development of cavitation in a centrifugal pump. Vibration signals are analyzed in the frequency and time–frequency domains. An ameliorative time–frequency algorithm based on the short time Fourier transform (STFT) and Wigner–Ville distribution (WVD) is proposed in this paper. The remainder of this paper is arranged as follows. First, brief descriptions of the time–frequency approaches are presented. The main purpose of this study is to obtain an experimental diagnostic approach for cavitation processes. Second, a typical kinetic pump under cavitation conditions is detected, and the relationship between vibration signals and suction performance of a centrifugal pump is analyzed. Finally, the time–frequency characteristics of unsteady cavitation phenomena are investigated. The results shows that a narrowband frequency range of vibration signals correlates well with typical critical cavitation condition and can be used to analyze the degree of pump cavitation.

2. Brief descriptions of time–frequency algorithms

Vibration signals were analysed in the frequency and time–frequency domains by using MATLAB in this study. A time–frequency analysis was conducted by the WVD, STFT and the proposed STFT–WVD method to provide information about their time evolution.

2.1 Wigner–Ville distribution

The WVD method is one of the most basic time-frequency distribution method. For the linear frequency modulation (LFM), hyperbolic FM or sinusoidal FM signal, the WVD method can be detected effectively. The Wigner–Ville distribution of the signal $x(t)$ is defined as Fourier transform of instantaneous autocorrelation of $x(t)$, as follows:

$$WVD_x(t,f)=\int_{-\infty}^{\infty}x\left(t+\frac{\tau}{2}\right)x^*\left(t-\frac{\tau}{2}\right)e^{-j2\pi f\tau}d\tau \tag{1}$$

where x(t) is a linear addition of a number of $x_i(t)$, i = 1, 2,…($x(t)=\sum_i x_i(t)$), the integrand of WVD ($x\left(t+\frac{\tau}{2}\right)x^*\left(t-\frac{\tau}{2}\right)$) is called instantaneous autocorrelation function of WVD (denoted by $r_x(t,\tau)$).

By definition, the WVD belongs to the two-type transformation and does not satisfy the superposition principle. For the two components of the signal, that is, $x(t) = x_1(t)+ x_2(t)$, the result of the WVD is as follows:

$$WVD_x=WVD_{x_1}+WVD_{x_2}+WVD_{x_1x_2}+WVD_{x_2x_1} \tag{2}$$

where WVD_{x_1} and WVD_{x_2} are the signal terms, and $WVD_{x_1x_2}$ and $WVD_{x_2x_1}$ are the cross terms. $r_x(t,\tau)$ can be considered as a signal containing additive noise. The WVD of the signal $x(t)$ is equal to the sum of the self–Wigner–Ville distribution of each signal $x_i(t)$, and the real part of their cross Wigner-Ville distribution. The cross term of the WVD is unavoidable. The cross terms become significantly severe to distinguish them from signal terms when the signal terms increase gradually.

In order to explain the character of the cross terms intuitively, the signal $x(t)$ is introduced which consists of two parts. The signal $x(t)$ is as follows:

$$x_1(t)=\cos(2\pi*200t),(0\le t\le 0.8) \tag{3}$$

$$x_2(t)=\cos(2\pi*50t),(0.2\le t\le 1) \tag{4}$$

$$\mathrm{x}(t)=x_1+x_2\ . \tag{5}$$

Fig. 1(a) depicts the time domain diagram of the signal $x(t)$. The result of the WVD of the signal $x(t)$ is shown in Fig. 1(b). When the frequency is 50 Hz or 200 Hz, it is the self-Wigner-Ville distribution of the signal component. The cross interference terms exist between 50 Hz to 200 Hz as marked by red dotted line. The notable characteristic of cross terms is the oscillation fluctuation from positive to negative. When the cross terms are serious enough, the signal terms will be overwritten, the authenticity of the original signal will also be affected. Thus, these cross terms influence the authenticity of the original signal.

2.2 United algorithm of STFT–WVD

According to the description of the WVD method mentioned above, the inner product of the cross term and the signal term is approximate to zero, which means the self-Wigner-Ville distribution is uncorrelated with the cross interference term. Therefore, an ideal template $r_M(t,\tau)$, is required to achieve the distribution.

STFT is a commonly used time-frequency analysis tool for the time-varying characteristics of non-stationary signal. We set the time continuous signal for analysis to s(t). The window function is g(t), and the signal of the STFT is defined as follows:

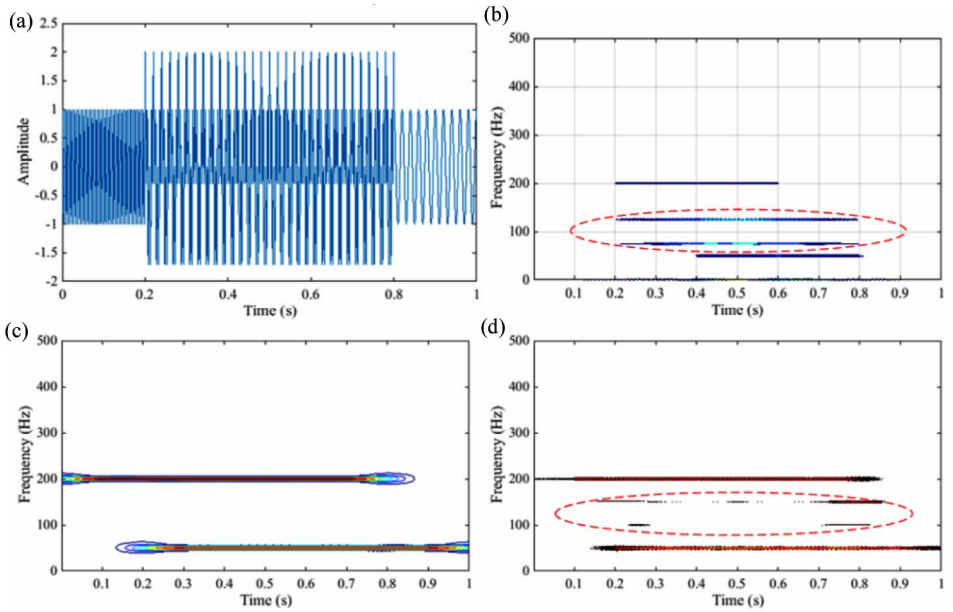

Fig. 1. The time domain diagram and the calculation result of three algorithms of the signal $x(t)$: (a) The time domain diagram of signal $x(t)$; (b) the calculation result of WVD method; (c) the calculation result of STFT method; (d) the calculation result of STFT-WVD method.

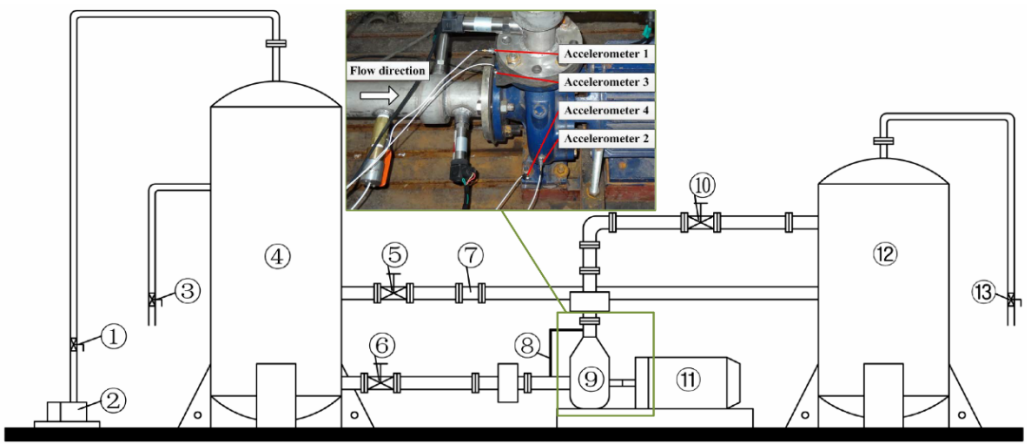

Fig. 2. Closed test rig at NRCP (1, 3, 13: ball valve; 2: vacuum pump; 4: pressure tank; 5, 10: butterfly valve; 6: gate valve; 7: turbine flowmeter; 8: static pressure transmitter; 9: test pump; 11: electromotor; 12: buffer tank. Not scale).

$$STFT_S(t,f)=\int_{-\infty}^{\infty}s(\tau)g^*(\tau-t)e^{-j2\pi f\tau}d\tau \tag{6}$$

where g(t) is a function with a short time width along the time axis. Thus, the STFT can be considered on the basis of the Fourier transform of the signal s(t) near the analysis time t which is commonly referred to as the 'local spectrum'.

Fig. 1(c) shows the result of the STFT of the signal $x(t)$, the spectrum indicate the regularity of the frequency content with time. By definition, the STFT belongs to a linear transform and consequently lacks the cross term for multi-component signals. It can be found that there is no cross terms in the spectrogram. It is believed that STFT is related to the self-Wigner-Ville distribution and is uncorrelated to the cross interference term. Therefore, the STFT conforms to the selection condition of the ideal template ($r_M(t,\tau)$).

Set $WVD_M(t,\omega)=\left|STFT(t,\omega)\right|^2$, the expression of Wigner-Ville distribution will be as follows:

$$WVD_{x,a}(t,\omega)=WVD_x(t,\omega)\left|STFT(t,\omega)\right|^2. \tag{7}$$

Eq. (7) is the principle expression based on the united algorithm of STFT and WVD.

Fig. 1(d) shows the result of STFT-WVD of the signal x(t), compared with the distribution of WVD, it can be found that the cross terms are basically eliminated, which reduces the influence on the original signal terms greatly. Meanwhile, the STFT-WVD retains an excellent time-frequency concentration

compared to the distribution of STFT. In addition, the existence of background noise is inevitable in acquiring of vibration signal data; in such case, denoising is commonly used to pre-process vibration signals [25]. In Fig. 1(d), the united algorithm can also eliminate the interference of background noise and is conducive to the monitoring and pre-processing of vibration signals.

3. Estimation of cavitation using vibration measurement

3.1 Experimental apparatus

An experiment platform should be set up to gather vibration signals under cavitation state. Experimental measurements were performed at the closed experimental rig of the National Research Centre of Pumps (NRCP) in China. Fig. 2 presents the schematic of the test equipment, which comprises three parts, namely, recycle water flow loop, model pump, and data acquisition equipment.

Water was stored in a 4.5 m^3 stainless steel reservoir tank. A rotary-vane vacuum pump was used to adjust the pressure inside the reservoir tank, and the flow rate was varied by the outlet butterfly valve and measured by a turbine flow-meter with an uncertainty of 0.2 % class. Both the suction and discharge average pressure signals were measured by piezoelectric pressure transducers with 0.25 % FS accuracy. The ranges of the sensors are -1 to 1 bar at the inlet and 0 to 6 bar installed at pump outlet. A 7.5-kW AC electromotor was used to drive the test pump. The rotational speed was measured by using a photoelectric tachometer. The fluid temperature was measured by PT100 temperature transducer with 0.12 % class. We used the piezoelectric vibration acceleration sensor MA352A60, which measures a range of 5–70 kHz and the sensitivity is 1000 mV/g. Four acceleration sensors were arranged on the pump body, inlet and outlet flanges and pump base. The specific installation is illustrated in Fig. 2. Vibration signals were gathered with a PXI-472B dynamic signal acquisition card obtained from the American NI Company. The DAQ assistant function in LabVIEW was applied to achieve vibration signal acquisition and display.

3.2 Overview of pump performance

A single-stage single-entry centrifugal pump was used as the test pump in this study. The pump characteristic curves are exhibited in Fig. 3. The pump was designed to operate at 2900 r/min with the volume flow rate Q_d = 60 m^3/h and the head H_d = 32 m. The specific speed is n_s = 101.6 at the designed point ($n_s = 3.65nQ^{0.5}H^{-0.75}/60$), and detail information about the parameters of the test pump can be obtained in the previous research [1]. For experimental cavitation, the vacuum pump was used to reduce the inlet pressure. Consequently, the vacuum degree of the pump suction increased. In the process of cavitation, the rotating speed and flow rate were fixed at constant values. In addition, the rotating speed was controlled by a frequency converter. The data of the cavitation tests for a flow range from 13 m^3/h to 65 m^3/h were gathered.

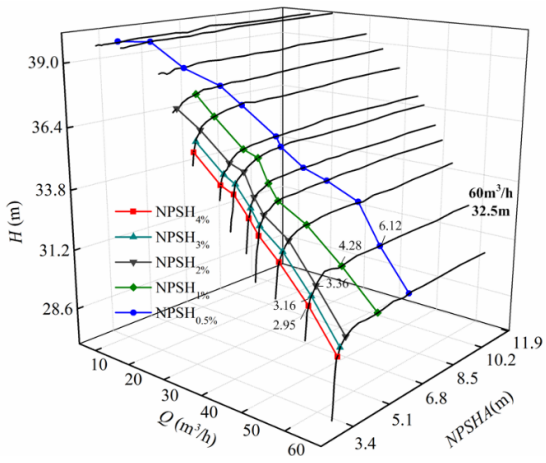

Fig. 3. Cavitation performance of the test pump at Q_d.

In Fig. 3, the curvilinear trends of the cavitation performance were nearly concordant under deep part load conditions. Moreover, the value of the required net positive suction head was 3.16 m at the design flow rate. This value was defined from the NPSHa value that corresponds to the 3 % head-drop. The cavitation was serious in the pump when the available net positive suction head (NPSHa) is lower than 3.16 m. Five NPSHa curves for % head drops (i.e. 0.5 %, 1 %, 2 %, 3 % and 4 %) at various flow rates are plotted in Fig. 3.

3.3 Pump cavitation evolution due to numerical method

Due to the evolution of the pump cavitation cannot be directly observed by the visualization method in the present experiment, the numerical simulation is used as an alternative for the qualitative analysis of the development of cavitation. Five conditions with different NPSHa values at Q_d are selected to clarify the relationship among the cavity evolution. Fig. 4 shows the distributions of the water vapour bubbles and turbulence kinetic energy at 0.7 span. Location of the impeller span is shown in Fig. 5 and was presented in our previous article [26]. As expected, the distribution of the turbulence kinetic energy is strongly correlated with the cavity development. In Fig. 4, no obvious vapour bubbles are found in the cavitation condition when NPSHa = 6.96 m. As the NPSHa decreasing to 5.93 m, partial cavity attaches to the suction side of the blade leading edge, which are especially in the impeller channel next to the volute tongue. With the cavitation intensifying, the cavity extends along the suction blade surface and then occurs in all blade leading edges. Meanwhile, the turbulent kinetic energy with higher values are developed in the zones downstream of the cavity closure. When the NPSHa drops to 3.04 m, the cavitation zone extends to the pressure surface and the turbulent kinetic energy distribution in the impeller channel are significantly altered. In this case, an evident head-drop phenomenon occurs.

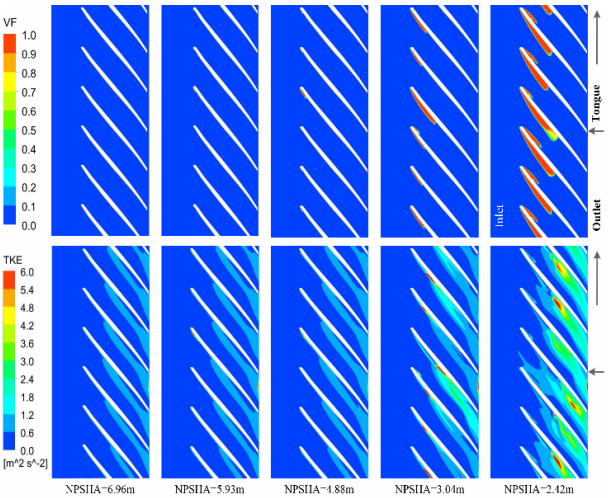

Fig. 4. Distribution of the vapour volume fraction (up) and the turbulent kinetic energy (down) in the blade-to-blade view at 0.7 span.

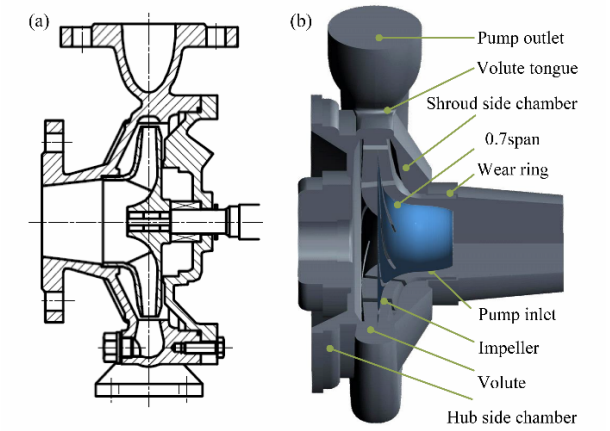

Fig. 5. Outline of the centrifugal pump: (a) Section view of the pump; (b) pump passage [26].

3.4 Relationship between vibration and suction performance

As mentioned above, when the NPSHa decreased from 11.34 m to 2.85 m, various cavitation stages from cavitating-free condition to cavitation breakdown condition were observed. Relation between the root mean squares (RMS) of vibration in different positions and the suction performance curve of the centrifugal pump can also be obtained during the development of cavitation, as shown in Fig. 6. In this figure, RMS/g ('g' is the gravitational acceleration) was adopted to define the dimensionless vibration, and the RMS is defined as:

$$RMS = \sqrt{\frac{1}{N}\sum_{k=1}^{N} X_k^2} \tag{8}$$

where N represents the total number of samples and X_k is the value of the vibration measured at a certain moment. Similar development trends emerged whilst cavitation progresses in accordance with the RMS signals of the vibration measured by four accelerometers. The RMS values of the measured

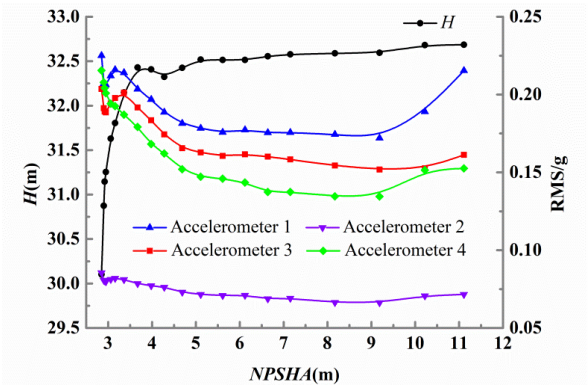

Fig. 6. Root mean square of vibration and suction performance curve.

vibration signals were higher in different positions than in steady state under a non-cavitation condition. The RMS values started to increase, and the head began to drop as the NPSHa decreased to 9.19 m. Then, the RMS signals maintained a relatively steady state with the decrease in the NPSHa from 7.15 m to 5.61 m.

The RMS values of the vibration signals increased quickly in the different positions, except those in accelerometer 2, as the NPSHa decreased to 5.11 m. The RMS values of the vibration signals increased sharply with the decrease in the NPSHa to 3.67 m with the cavitation constantly developed; meanwhile, the head of the centrifugal pump dropped dramatically. Incipient cavitation also occurred when the NPSHa declined to 5.11 m with the decrease in pump suction pressure, which can also be verified by Fig. 4. This condition could lead to an increase in vibration and to a drop in the pump head. The cavity volume increased quickly, and the liquid was extruded and gained elevated energy with the decrease in the NPSHA to 4.69 m. The expanding cavitation bubbles occupied a large part of the passage and obstructed the liquid in the impeller with a further decline in the NPSHa. This condition induced the sharp increase and dramatic drop of the head. The RMS values of the vibration signals slightly declined, as tested by accelerometers 1 and 3, with the decrease in the NPSHa to 3.36 m.

The RMS values of the vibration signals were larger when tested by accelerometers 1 and 3 than when tested by the other accelerometers. This phenomenon was due to the two accelerometers were positioned near the impeller. In particular, detecting the generation of cavitation was more suitable in these positions than in the positions of the other accelerometers. Moreover, the RMS values of the vibration signals were larger than when tested by accelerometer 4 than when tested by accelerometer 2. The primary reason was due to accelerometer 4 was installed on the pump base where accelerometer 4 gathered the vibration signals induced by not only the cavitation but also the whole mechanical system. This result also indicated that cavitation played a major role in the vibration compared with the mechanical system. The comparison of vibration intensity and the curve trend of the RMS revealed that the vibration signals tested by accelerometer 3 are suitable for

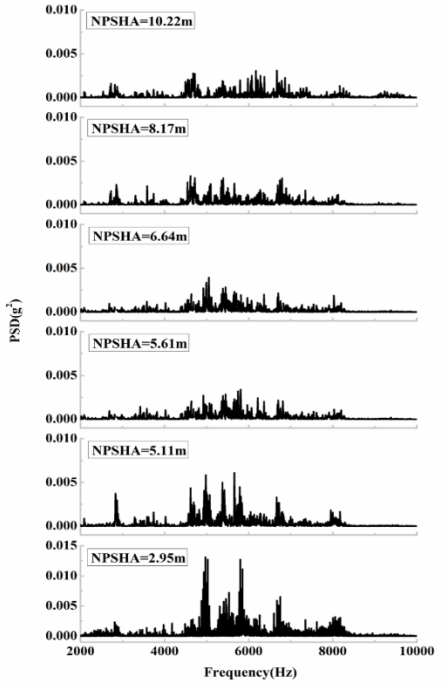

Fig. 7. PSD of vibration signals on the inlet flange at Q_d.

analysing the cavitation progress. The vibration signals tested at this position were used in the analysis conducted in the following study.

A detailed observation of the vibration signals is displayed in Fig. 7, which presents the results analysing the power spectral density (PSD) of the vibration signals. The broadband pulse of the vibration signals existed in the whole frequency range. The broadband pulse of the generated vibration signals ranged from 2 kHz to 10 kHz. The broadband pulsations of the vibration signals intensified, and the amplitude gradually increased with the development of cavitation. Broadband fluctuations slightly became severe when the NPSHa decreased to 5.11 m. The amplitude of the pulsations increased to approximately five times of that in the non-cavitation condition whilst the cavitation fully developed (NPSHa = 2.95 m). Furthermore, the broadband distribution concentrated between 4 and 8.5 kHz when the cavitation became severe. The vibration signals intensified when the attached cavitation bubbles shed from the blade leading edges and propagated to the outlet of the blade channels to occupy nearly the whole impeller. Then, the collapse of vapour bubbles produced shockwaves and pressure. In accordance with the PSD signals, the condition of NPSHa = 5.11 m can be regarded as the presence of cavitation.

4. Time–frequency characteristic of the unsteady cavitation phenomena

In this study, vibration signals were gathered under cavitation condition at the design flow rate. As a result of the random and discrete nature of the cavitation process, vibration signals were preferably analysed on the basis of time–frequency characteristics. This study adopted two analytical methods, namely, the STFT and STFT–WVD. The valuable information is presented as follows.

4.1 STFT

Fig. 8 shows the 3D map of the STFT. The colour in the figure indicates the peak of the value, the higher peak values of the time-frequency domain, the brighter the color. As the vibration signals did not change obviously in the time–frequency domain from 11.34 m to 6.12 m of the NPSHa, only the case of NPSHa = 6.64 m is presented in Fig. 8(a). The development of cavitation states was observed clearly when the value of NPSHa is less than 5.11 m. When the value of NPSHa was 2.95 m, the energy was aggregated, and the amplitude generally increased, which was two times higher than that in the normal state, as shown in Fig. 8(d). The reason for this phenomenon may be the content of vapour that rapidly increased and the load on the pump impeller decreased. This overall condition caused the amplitude to decrease rapidly. Moreover, cavitation had developed completely at this stage.

By definition, the STFT does not have any cross terms for multi-component signals. However, the time–frequency concentration is poor, and the peak is massive and lacks clear lines. This situation affects the time–frequency analysis of vibration signals, and only the gross distribution can be obtained. Moreover, incipient cavitation emerged in accordance with the experimental performance of the test pump when the value of NPSHa was 5.61 m or less. However, the distributions, including the amplitude and frequency content, did not change obviously, as shown in Fig. 8.

4.2 STFT–WVD

The calculation results of the STFT–WVD are exhibited in Fig. 9. The vibration signals obtained from the centrifugal pump consisted of two distinctive parts, that is, discrete components superimposed on a broadband background.

For the prediction based on the foregoing analysis, we concluded that the distribution of the STFT–WVD showed an excellent time–frequency aggregation. A high density equated to a large amplitude. The stage of the complete development of cavitation was easy to acquire, as illustrated in Figs. 9(a) and (d). The energy density distribution gradually enhanced and was concentrated in the high- and low-frequency domains when the value of NPSHa ranged from 5.61 m to 2.95 m. The energy showed a dense distribution as NPSHa = 2.95 m. Cavity increase quickly and the energy was aggregated. Furthermore, the vibration became intense, as analyzed by using the STFT, and the cavitation became fully developed under this condition. This result was due to the pulse of the bubble collapsed in the flow that strengthened the vibration in the pump.

The calculation results of the united algorithm were similar to those of the results obtained with the STFT under the state of incipient cavitation. However, the united algorithm differed

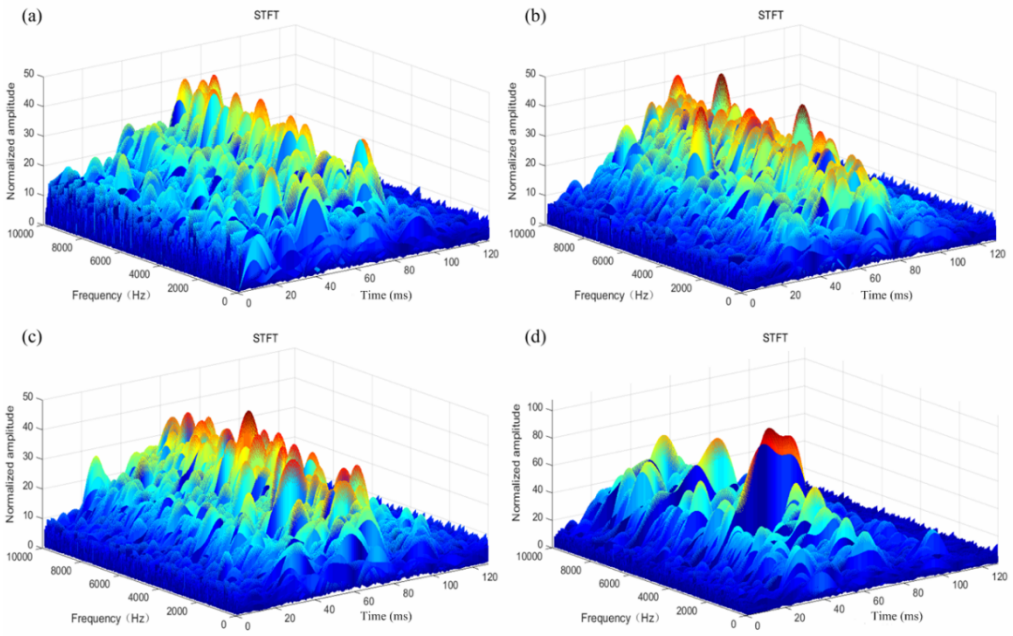

Fig. 8. Calculation results of three-dimensional maps of the STFT at Q_d: (a) NPSHa = 6.64 m; (b) NPSHa = 5.61 m; (c) NPSHa = 5.11 m; (d) NPSHa = 2.95 m.

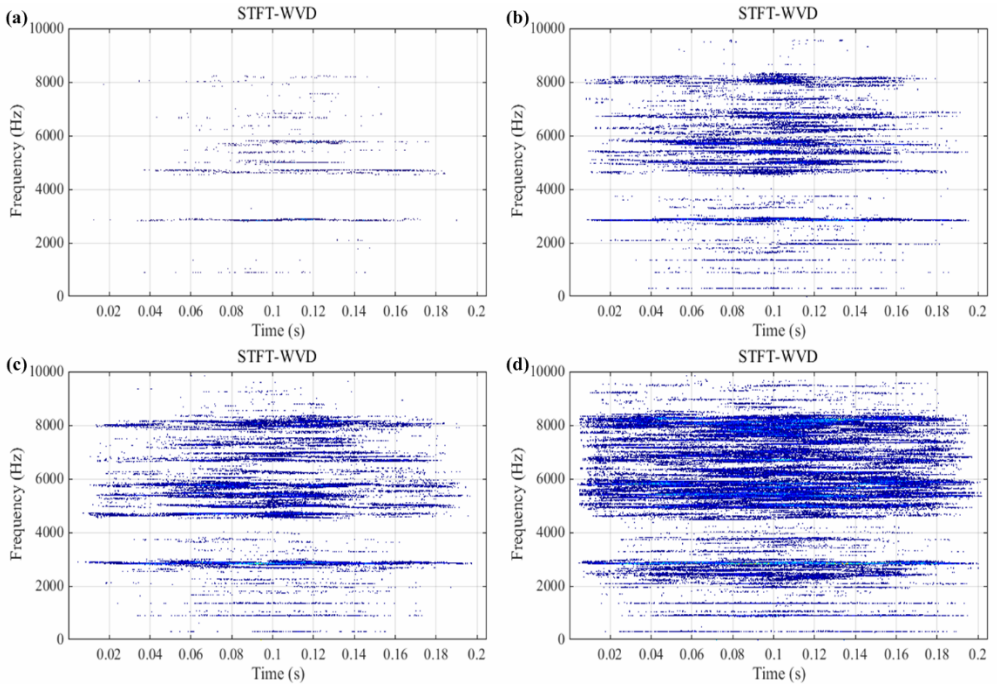

Fig. 9. Calculation results of the STFT–WVD at Q_d: (a) NPSHa = 6.64 m; (b) NPSHa = 5.61 m; (c) NPSHa = 5.11 m; (d) NPSHa = 2.95 m.

from the previous result because this algorithm allowed the extraction of estimable information. A slight change in the distribution was obtained at the developing state of cavitation, as shown in Fig. 9(c). The frequency content did not change, but the energy density became more slightly concentrated than that at the onset of cavitation. Incipient cavitation was initiated in accordance with the experimental performance of the test pump when the value of the NPSHa was 5.61 m or less. The distributions of normal state and incipient cavitation are compared and plotted in Figs. 9(a) and (b). The energy density, amplitude, and frequency content changed overtly. The distribution was particularly concentrated in the high frequency area from 6 kHz to 8.5 kHz. Thus, the onset of cavitation was verified when the value of the NPSHa was 5.61 m. This state entered earlier than the PSD signals (also earlier than 3 % head drop). So the united algorithm can supply an effective

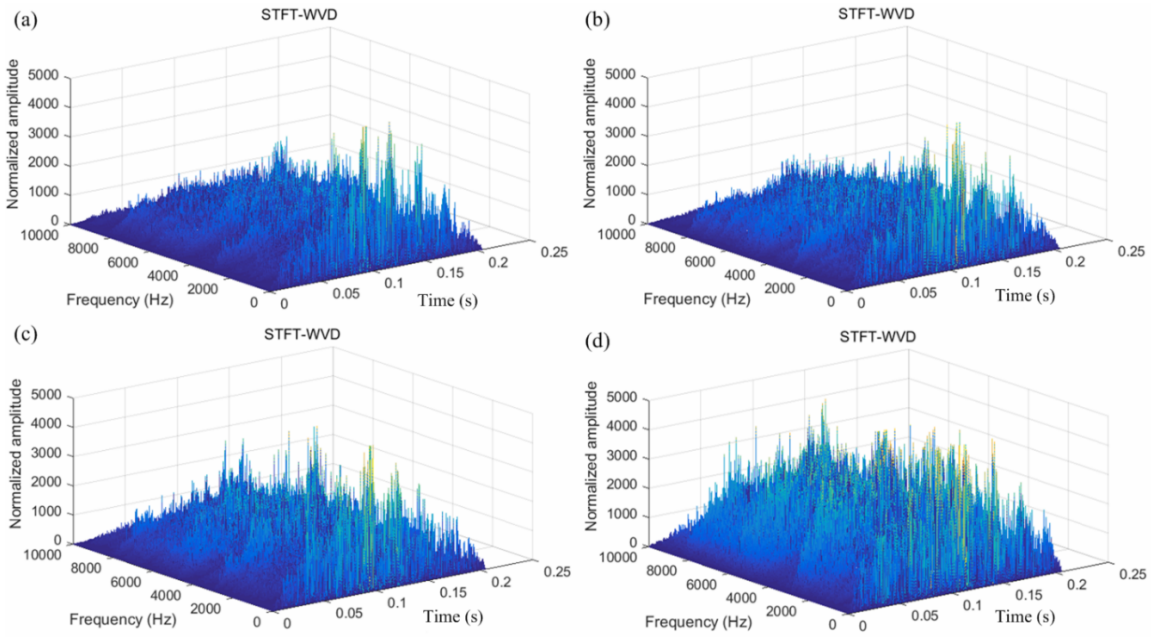

Fig. 10. Calculation results of three-dimensional maps of the STFT–WVD at Q_d: (a) NPSHa = 6.64 m; (b) NPSHa = 5.61 m; (c) NPSHa = 5.11 m; (d) NPSHa = 2.95 m.

solution.

A display of the waterfall plot was useful in explaining the process of incipient cavitation. Fig. 10 displays the 3D map of the calculation results of the STFT–WVD. Four cavitation states showed that the vibration signal strengthened with the decrease in the head drop. As shown in Figs. 10(a) and (b), the calculation results with the cavitation process were similar, particularly when the NPSHa ranged from 6.64 m to 5.61 m. However, changes were observed in the process of incipient cavitation during the course of transition. The vibration signals were mostly concentrated in the high-frequency components in the normal state. Thereafter, intermediate frequency components started to fluctuate, especially at approximately 6000 Hz. This result indicated that the state of cavitation inception began to form. These differences were sufficiently significant for allowing the use of the STFT–WVD to detect the onset of cavitation and prevent further cavitation in the centrifugal pump by initiating an alarm.

Besides, the signal intensity, amplitude, and energy distribution were nearly twice as high as those in other cavitation states as shown in Fig. 10(d). Cavitation was fully developed in this state when the value of the NPSHa was around 2.95 m. This area was consistent with the experimental performance of the test pump with a head drop area of 4 %. The hydraulic instability was severe in this regime, indicating the need for high energy to surmount the regime.

5. Conclusions

In this work, an experimental investigation was conducted to gather the vibration signals induced by the development of cavitation in a centrifugal pump. The vibrations and instabilities induced by cavitation in a centrifugal pump were investigated during the development of cavitation. The results revealed the obvious corresponding relationship between the development of cavitation and the intensification of vibration with the decrease in the NPSHa.

Compared with the distribution of the STFT and WVD, the united algorithm (STFT–WVD) retained a useful time–frequency concentration and eliminated the interference of the cross terms. A study on the STFT and united algorithm STFT–WVD was conducted to analyze the vibration signals for monitoring the states of cavitation. The time–frequency analysis method of the STFT was used to identify cavitation states. In accordance with the experimental performance of the test pump, these characteristics indicated that the algorithm of the STFT for monitoring vibration signals can be used as a confirmation of the existence of cavitation but not its onset. The time–frequency characteristics of the STFT–WVD revealed several differences from those of the STFT. The distribution was concentrated heavily in the high area from 6 kHz to 8.5 kHz. The intermediate frequency components of approximately 6 kHz fluctuated for the first time with the formation of incipient cavitation. Thus, this condition was regarded as an indicator for detecting the onset of pump cavitation.

Acknowledgments

This work was supported by the National Natural Science Foundation of China (Grant No. 51776189, 51536008), Zhejiang Provincial Natural Science Foundation (Grant No. LZ15E090002), and Key Research and Development Program of Zhejiang Province (Grant No. 2017C01021). The supports are gratefully acknowledged.

Nomenclature

STFT	: Short time Fourier transform (–)
WVD	: Wigner–Ville distribution (–)
LFM	: Linear frequency modulation (–)
$s(t)$	: Time continuous signal (–)
$g(t)$	: Window function (–)
$x(t)$	: Analytical form of signal (–)
$r_x(t,\tau)$	: Instantaneous autocorrelation function of WVD (–)
$r_M(t,\tau)$	: Ideal template (–)
D_s	: Pump inlet diameter (mm)
D_0	: Pump outlet diameter (mm)
D_1	: Impeller inlet diameter (mm)
D_2	: Impeller outlet diameter (mm)
b_2	: Blade width at exit (mm)
Z	: Blade number (–)
D_3	: Volute tongue diameter (mm)
Q_d	: Design flow rate (m^3/h)
H_d	: Design head (m)
n	: Rotational speed (r/min)
NPSHr	: Required net positive suction head (m)
NPSHa	: Available net positive suction head (m)
RMS	: Root mean squares (–)
N	: Total number of samples (–)
X_k	: Value of the vibration measured (–)
PSD	: Power spectral density (–)

References

[1] X. J. Li, B. X. Yu, Y. C. Ji, J. X. Lu and S. Q. Yuan, Statistical characteristics of suction pressure signals for a centrifugal pump under cavitating conditions, *Journal of Thermal Science*, 26 (1) (2017) 47-53.

[2] H. Li, B. Yu, B. Qing and S. R. Luo, Cavitation pulse extraction and centrifugal pump analysis, *Journal of Mechanical Science and Technology*, 31 (3) (2017) 1181-1188.

[3] J. Černetič, The use of noise and vibration signals for detecting cavitation in kinetic pumps, *Proceedings of the Institution of Mechanical Engineers Part C: Journal of Mechanical Engineering Science*, 223 (7) (2009) 1645-1655.

[4] X. L. Fu, D. Y. Li, H. J. Wang, G. H. Zhang, Z. G. Li and X. Z. Wei, Analysis of transient flow in a pump-turbine during the load rejection process, *Journal of Mechanical Science and Technology*, 32 (5) (2018) 2069-2078.

[5] W. Yang, R. F. Xiao, F. J. Wang and Y. L. Wu, Influence of splitter blades on the cavitation performance of a double suction centrifugal pump, *Advances in Mechanical Engineering*, 6 (2014) ID 963197.

[6] M. Čudina, Detection of cavitation phenomenon in a centrifugal pump using audible sound, *Mechanical Systems and Signal Processing*, 17 (6) (2003) 1335-1347.

[7] M. Čudina and J. Prezelj, Detection of cavitation in operation of kinetic pumps. Use of discrete frequency tone in audible spectra, *Applied Acoustics*, 70 (4) (2009) 540-546.

[8] X. W. Luo, B. Ji and Y. Tsujimoto, A review of cavitation in hydraulic machinery, *Journal of Hydrodynamics*, 28 (3) (2016) 335-358.

[9] X. M. Guo, L.H. Zhu, Z. C. Zhu, B. L. Cui and Y. Li, Numerical and experimental investigations on the cavitation characteristics of a high-speed centrifugal pump with a splitter-blade inducer, *Journal of Mechanical Science and Technology*, 29 (1) (2015) 259-267.

[10] J. X. Lu, S. Q. Yuan, Y. Luo, J. P. Yuan, B. L. Zhou and H. Sun, Numerical and experimental investigation on the development of cavitation in a centrifugal pump, *Proceedings of the Institution of Mechanical Engineers Part E Journal of Process Mechanical Engineering*, 23 (4) (2014) 1989-1996.

[11] J. X. Lu, S. Q. Yuan, P. Siva, J. P. Yuan, X. D. Ren and B. L. Zhou, The characteristics investigation under the unsteady cavitation condition in a centrifugal pump, *Journal of Mechanical Science and Technology*, 31 (3) (2017) 1213-1222.

[12] M. Chudina, Noise as an indicator of cavitation in a centrifugal pump, *Acoustical Physics*, 49 (4) (2003) 463-474.

[13] M. Ashokkumar, The characterization of acoustic cavitation bubbles - An overview, *Ultrasonics Sonochemistry*, 18 (4) (2011) 864-872.

[14] H. S. Han, K. H. Lee and S. H. Park, Evaluation of the cavitation inception speed of the ship propeller using acceleration on its adjacent structure, *Journal of Mechanical Science and Technology*, 30 (12) (2016) 5423-5431.

[15] S. Christopher and S. Kumaraswamy, Identification of critical net positive suction head from noise and vibration in a radial flow pump for different leading edge profiles of the vane, *ASME Journal of Fluids Engineering*, 135 (12) (2013) 121301.

[16] A. T. Faisal, The non-intrusive detection of incipient cavitation in centrifugal pumps, *Ph.D. Thesis*, University of Huddersfield, Huddersfield (2011).

[17] P. Harihara and A. Parlos, Sensorless detection of impeller cracks in motor driven centrifugal pumps. *Proceedings of the 2008 International Mechanical Engineering Congress and Exposition*, Boston, USA, October 31-November 6 (2008).

[18] K. K. Mckee, G. L. Forbes, I. Mazhar, R. Entwistle, M. Hodkiewicz and I. Howard, A vibration cavitation sensitivity parameter based on spectral and statistical methods, *Expert Systems with Applications*, 42 (1) (2015) 67-78.

[19] J. Černetič and M. Čudina, Estimating uncertainty of measurements for cavitation detection in a centrifugal pump, *Measurement*, 44 (7) (2011) 1293-1299.

[20] Y. Wen and M. P. Henry, Time frequency characteristics of the vibroacoustic signal of hydrodynamic cavitation, *Journal of Vibration and Acoustics*, 124 (4) (2002) 469-475.

[21] Y. Feng, B. C Lu and D. F. Zhang, Multiscale singular value manifold for rotating machinery fault diagnosis, *Journal of Mechanical Science and Technology*, 31 (1) (2017) 99-109.

[22] M. R. Hodkiewicz and M. P. Norton, The effect of change in flow rate on the vibration of double suction centrifugal pumps, *Proceedings of the Institution of Mechanical Engi-*

neers Part E Journal of Process Mechanical Engineering, 216 (1) (2002) 47-58.

[23] G. Cavazzini, G. Pavesi and G. Ardizzon, Pressure instabilities in a vanned centrifugal pump, *Proceedings of the Institution of Mechanical Engineers Part A: Journal of Power and Energy*, 225 (7) (2011) 930-939.

[24] G. Pavesi, G. Cavazzini and G. Ardizzon, Time-frequency characterization of the unsteady phenomena in a centrifugal pump, *International Journal of Heat and Fluid Flow*, 29 (5) (2008) 1527-1540.

[25] E. Grist, *Cavitation and the centrifugal pump: A guide for pump users*, FL: CRC Press (1998).

[26] X. J. Li, Z. C Zhu, Y. Li and X. P. Chen, Experimental and numerical investigations of head-flow curve instability of a single-stage centrifugal pump with volute casing, *Proceedings of the Institution of Mechanical Engineers Part A: Journal of Power and Energy*, 230 (7) (2016) 633-647.

Xiaojun Li received his B.S. degree from Zhengzhou University in 2008, and his M.S. and Ph.D. degrees in Fluid Machinery and Engineering from Jiangsu University in 2010 and 2013, respectively. He is currently an Assistant Professor in Zhejiang Sci-Tech University, China.